Effect of Cr Concentration on ½<111> to <100> Dislocation Loop Transformation in Fe-Cr alloys

Yaxuan Zhang, Ziqi Xiao, Xian-Ming Bai*

Department of Materials Science and Engineering, Virginia Polytechnic Institute and State University, Blacksburg, VA 24061, United States

Abstract

Radiation can produce both <100> and ½<111> type dislocation loops in Fe-Cr based ferritic/martensitic alloys. However, contradictory experimental results have been reported on how Cr concentration affects the ratio of <100> to ½<111> loops. In this study, firstly molecular dynamics simulations are conducted to study how Cr concentration affects the formation probability of <100> loops from overlapping cascades on a pre-existing ½<111> loop in a series of Fe-Cr alloys with 0 - 15%Cr at 300 K using a concentration-dependent interatomic potential. Our atomistic modeling directly demonstrates that the ratio of <100> to ½<111> loops decreases with the increasing Cr concentration, which is consistent with many experimental observations. Next, independent molecular statics calculations show that the formation energy of a <100> loop has a much faster increase rate than that of a ½<111> loop as Cr concentration increases, indicating that the formation of <100> loops becomes energetically more and more unfavorable than ½<111> loops as the Cr content increases. Using a different interatomic potential, the Cr dependence on the <100> loop formation probability is weak, because this potential predicts that Cr addition does not change the relative energy difference between <100> and ½<111> loops. Our results provide an alternative explanation for why Cr can suppress the formation of <100> loops in Fe-Cr alloys, which can be applied to all <100> loop formation mechanisms. The possible effects of other alloying elements on the formation of <100> loops in Fe-based alloys are also discussed.

Keywords: Radiation damage, <100> and ½<111> dislocation loops, molecular dynamics, Fe-Cr alloys, Cr concentration dependence.

*Corresponding author.

Email address: xmbai@vt.edu (X.M. Bai)

1. Introduction

Iron-chromium (Fe-Cr) based ferritic/martensitic (F/M) alloys are leading candidate structural and cladding materials for next-generation fission and fusion nuclear reactors [1]. Compared to their austenitic stainless steel counterparts, Fe-Cr based F/M alloys have higher thermal conductivities, lower coefficients of thermal expansion, and better void swelling resistance [2-5]. However, radiation can still induce complex microstructural evolution in Fe-Cr alloys, such as formation of interstitial-type dislocation loops [6], radiation-induced segregation of alloying elements at defect sinks [7], and precipitation of the Cr-rich α ' phase [8, 9]. In particular, the formation of dislocation loops and α' precipitates can impede dislocation motion [10-12], leading to radiation hardening and embrittlement. Dislocation loops can be directly produced by displacement cascades [13-15], or form due to the accumulation of interstitials [16]. Unlike many other body-centered-cubic (BCC) metals in which the Burgers vector of interstitial dislocation loops is predominately $\frac{1}{2}$ <111>a (where a is the lattice constant), dislocation loops with Burgers vectors of both $\frac{1}{2}$ <111>a and <100>a have been found in pure Fe and Fe-Cr alloys [15, 17-28]. The two types of dislocation loops have distinct properties such as mobility. In general, ½<111> (sometimes referred as "<111>" for simplicity in this work) type dislocation loops are glissile in the Burgers vector direction [29] so that they can migrate to defect sinks. In contrast, <100> type dislocation loops are much less mobile (sessile). As a result, they can serve as stationary defect sinks and impede dislocation motion [10].

In Fe-Cr alloys, formation of two types of dislocation loops under irradiation depends on both temperature and Cr content, as well as irradiation particle type and dose. In pure Fe, it has been shown in a self-ion irradiation experiment [24] that the predominate loop type is ½<111> when the irradiation temperature is below 300 °C and <100> if the temperature is above 500°C, respectively. The transition temperature is about 400 °C. The temperature dependence of the relative stability between two loop types has been interpreted as a result of reduction of shear stiffness constant (C'= $(C_{11}-C_{12})/2$) with the increasing temperature [30]. The effect of Cr content on the relative abundance of the two loop types has been studied in many irradiation experiments [25, 26, 28, 31-34], but contradictory results have been reported. Many experimental results have shown that the increasing Cr content suppresses the formation of <100> loops [25, 26, 28, 31], which are summarized as follows. Porollo et al. [26] showed that the predominant loop type was <100> when the Cr concentration was less than 6% (including pure Fe) under neutron irradiation to a dose of 5.5 –7.1 dpa (displacement per atom) at 400°C. When the Cr concentration was high (12%, 18%), both ½<111> and <100> loop types were observed, indicating that the formation potency of <100> loops decreases with the increasing Cr content. Similarly, Gelles [28] showed that both loop types were observed in a series of Fe-Cr alloys under neutron irradiation of 20 dpa at 400 - 450°C. The predominate loop type was <100> in Fe-3%Cr but ½<111> in Fe-12%Cr. Matijasevic et al. [25] compared the dislocation loop population in pure Fe and Fe-15%Cr single crystals under neutron irradiation to a low irradiation dose of 0.2 dpa at 300°C. Their results showed that <100> loops were predominant in pure Fe but no visible loops were observed in the Fe-15%Cr alloy, suggesting that Cr may suppress the formation of both types of loops. In a recent experiment of Kr⁺⁺ ion irradiation on a series of FeCrAl alloys to a dose of 2.5 dpa at 320°C by Haley et al. [31], the results showed that the fraction of ½<111> loops increased from 50% to 80% when the Cr content increased from 10% to 15%. In other words, the appearance frequency of <100> loops decreased with the increasing Cr content, although the presence of Al may also play a role on the outcome. In general, all these experimental studies have shown that the formation of <100> loops becomes more difficult as the Cr content increases, although scattered exceptions (such as the Fe-18%Cr-3%Al sample in Ref. [31]) exist. However, in some other experimental studies such a correlation was not very evident or an opposite trend was observed. For instance, Xu et al. [33] used Fe⁺ ions to irradiate pure Fe and a series of Fe-Cr alloys to a dose of 1 dpa at 300 °C. They reported that the <100> loop fraction in Fe-Cr alloys is higher than that in a pure Fe, which is opposite to the trend observed in aforementioned studies. Prokhodtseva et al. [32] conducted dual beam (Fe + helium) irradiation on pure Fe and Fe-Cr alloys to a dose of 1 dpa at room temperature. They concluded that Cr had a weak effect on the relative abundance of the two loop types but helium had a strong effect on suppressing the formation of <100> loops. In a recent follow-up study by some of these authors [34], they reported that the presence of Cr may either "frustrate" or sometimes even "favour" the formation of <100> loops, depending on the irradiation dose and temperature.

On the modeling side, the studies to date were mainly focused on understanding the formation mechanisms of <100> loops in pure BCC Fe using theoretical and atomistic modeling including molecular dynamics (MD) simulations. Several mechanisms have been proposed, which are briefly summarized as follows. (1) A shear in the <110> direction can transform a faulted <110> loop (enclosing a stacking fault) into a <100> loop at elevated temperatures [17]; (2) Two gliding ½<111> dislocation loops of similar sizes and overlapping gliding cylinders can interact with each other to form either a <100> or ½<111> loop [18, 19]. This mechanism has been extended to the reaction between three ½<111> loops [35], which may not require similar loop sizes; (3) A ½<111> loop can transform into a <100> loop at elevated temperatures by rearranging and reorienting crowdion clusters [21], because a <100> loop may be energetically more favorable than a $\frac{1}{2}$ <111> loop at high temperatures due to the reduction of shear stiffness constant [30]; (4) Transformation of C15 clusters, which can form directly from displacement cascades [13], into either <100> or ½<111> loops when a C15 cluster exceeds a critical size [22]; (5) Formation of <100> loops directly from very high-energy displacement cascades [15]; (6) Formation of <100> dislocation loops when displacement cascades overlap with pre-existing ½<111> loops or cascade debris [20, 23, 36-39]. Currently there is no consensus on which mechanism is the predominant one. It is likely that multiple mechanisms can be operative concurrently because they do not contradict each other. For the effects of alloving elements such as Cr on the formation of <100> type loops, very limited computational work has been conducted. Béland et al. [40] simulated the reaction of two nearly identical ½<111> loops in an Fe-10%Cr alloy using the self-evolving atomistic kinetic Monte Carlo (SEAKMC) method [19]. They found that the activation energy for formation of a <100> loop is statistically similar between pure Fe and Fe-10%Cr. Interestingly, the formation probability of <100> loops strongly depends on the spatial distribution of Cr atoms in the two initial ½<111> loops. In addition, they also predicted that the formation of ½<111> loops is likely more favorable than <100> loops in Fe-10%Cr because Cr may impede the reorientation of some crowdions. Granberg et al. [23] conducted MD simulations of continuous cascades in a pure Fe and an Fe-20%Cr alloy. They observed that <100> loops can form from overlapping cascades on the existing damage debris in both systems. They indicated that the addition of Cr does not affect the production frequency of the <100> loops. However, no detailed statistics was provided to directly support this claim.

From the aforementioned experimental studies, it can be seen that conflicting results exist regarding the effect of Cr on the formation probability of <100> loops in Fe-Cr alloys. Part of the reason may be that the formation of dislocation loops depends on irradiation conditions as well as the presence of other alloying elements in experiments. It may be also due to the loss of

mobile ½<111> loops to defect sinks before they are counted, which may lead to an artificially relative predominance of two loop types. This effect may become more pronounced in the *in-situ* ion irradiation with transmission electron microscopy (TEM) observation experiments in which ½<111> loops could easily escape to the free surfaces of thin TEM foils. On the modeling side, to our best knowledge very limited studies [23, 40] have been conducted to understand how Cr content influences the formation probability of <100> loops in Fe-Cr alloys. Therefore, the objectives of this work are two folds. First, we will conduct MD simulations to study how the Cr concentration influences the formation probability of <100> loops in pure Fe and a series of Fe-Cr alloys based on the mechanism #6 discussed above (i.e., cascade overlapping with a preexisting ½<111> loop). In each set of comparisons regarding the Cr effect, the simulations will be conducted under the same conditions except for the Cr concentration in order to minimize the factors that could affect the results. The correlation between Cr content and the potency of <100> loop formation (either promotion, suppression, or no effect), which has not been clearly established to date, will be elucidated. Second, if a correlation can be established, the underlying mechanism will be explored to provide a physically sound explanation for why such a correlation exists.

2. Methods

In this work, the LAMMPS [41] software is used to conduct MD simulations of cascade overlapping on a pre-existing ½<111> loop in both pure Fe and Fe-Cr alloys at 300 K. Previously, researchers have shown that the Burgers vector of an interstitial dislocation loop can change from $\frac{1}{2}$ <111>a to <100>a (or vice versa) or remain unchanged in pure Fe in such cascade overlapping simulations [20, 23, 36-39]. It should be noted that the purpose of our work is not to prove if this ½<111> to <100> loop transformation mechanism is the most probable one among the six mechanisms discussed above. Instead, it is used as a convenient and feasible method to determine how Cr concentration influences the formation probability of <100> loops in Fe-Cr alloys in the MD accessible timescale. The systems studied in this work include pure Fe, Fe-2%Cr, Fe-5%Cr, Fe-10%Cr, and Fe-15%Cr, all in atomic percent. The concentrationdependent embedded atom method (CD-EAM) potential developed by Stukowski et al. [42] is primarily used to describe the interatomic interactions. This CD-EAM potential correctly predicts the change of sign in the heat of mixing from negative to positive at around 10%Cr [43, 44], which is consistent with the DFT results [45]. In addition, the potential also correctly predicts that a <110> Fe self-interstitial atom (SIA) dumbbell is more stable than a <111> SIA dumbbell in pure Fe and a Cr atom has a positive binding energy with an Fe SIA [44], which are consistent with many DFT calculations [46, 47]. The potential of the Fe component in this CD-EAM potential was originally developed by Mendelev et al. (commonly referred as "M03" potential) [48], which has been successfully used to model <100> and ½<111> loops in pure Fe [20, 22, 35]. To check if the effect of Cr on loop formation depends on the choice of interatomic potential, the two-band model (2BM) potential developed by Bonny et al. [49] is also used (referred as "Bonny2011" potential in this work). The Fe-Fe component in this 2BM potential is the same as the M03 potential. This potential also predicts a reasonable heat of mixing curve. Note that both potentials cannot capture the temperature-dependent relative stability between the two loop types (i.e., ½<111> loop is more stable at low temperature while <100> loop is more stable at high temperature as observed in experiments [24]). Therefore, the temperature effect is not studied here and all the cascade overlapping simulations by MD are conducted at 300 K. Same as in our previous cascade simulations in Fe-based alloys [44, 50], the Ziegler-BiersackLittmark (ZBL) potential [51] is used to describe the strong short-range repulsive interactions between atoms when they become too close during the thermal spike. All the pair interaction terms in this potential are splined to the ZBL potential at 1.2 Å.

In each simulation system, the total number of atoms is 54,000 before a loop is introduced. The simulation box has a cubic geometry and the box length is $30a_0$, where a_0 = 2.86Å is lattice constant at 300 K for BCC Fe predicted by the M03 potential. Periodic boundary conditions are employed in all three Cartesian directions. To introduce a pre-existing ½<111> interstitial loop, a circular ½<111> dislocation loop is inserted at the center of the simulation box. In most simulations, the loop has a radius of 8Å and contains 35 interstitials. The habit plane for the ½<111> loop is {110} because many previous MD simulations [18, 22] have shown that it is the preferred habit plane in BCC Fe, although experimentally habit planes of {110}, {111}, {211} were all observed [21]. The Fe-Cr alloy systems are created by randomly distributing Cr atoms as substitutional atoms after a ½<111> loop is created. This procedure is conducted for each simulation at each Cr concentration in order to introduce stochastic effect on the Cr distribution in the initial configuration. Upon relaxation, the loop has a $\frac{1}{2} < 111 > a$ Burgers vector, as shown in Fig. 1(a). Here the dislocation extraction algorithm (DXA) method implemented in the OVITO software [52-54] is used to characterize the Burgers vectors of dislocation loops. In each cascade overlapping simulation, initially the simulation system is equilibrated at 300 K in a NPT ensemble (constant number of atoms, pressure, and temperature) for about 10 ps. Then an outer boundary layer with a thickness of 2.9Å is selected as the heat sink and the kinetic energies of atoms in this layer are controlled at 300 K by the velocity rescaling method. The rest of atoms are simulated in a NVE ensemble (constant number of atoms, volume, and energy). To initiate a recoil, an atom at about 14.5 Å below the center of the pre-existing ½<111> loop in z direction ([001] direction) is selected as the primary knock-on atom (PKA). The PKA direction is in the [001] direction so that the created cascade will have a good chance to overlap with the preexisting loop. The approximate position and direction of the PKA are illustrated in Fig. 1(a). The PKA energy is set to 2 keV, which can create a large-enough cascade to overlap with the preexisting ½<111> loop, as shown in Fig. 1(b). At this energy it was also shown previously that the effect of PKA direction on defect production became less pronounced [55]. After the PKA is initiated, the system is allowed to evolve for 22 ps in the NVE+sink ensemble and another 20 ps in a NPT ensemble. The final defect structure is analyzed using the DXA method. To get statistically meaningful results, 100 independent simulations are conducted for each Cr concentration using each potential. To check the effects of loop size, PKA energy, and PKA position on the loop formation, a larger pre-existing ½<111> loop containing 55 interstitials (~10 Å in radius) is also used. The PKA energy for the larger loop is 5 keV and the PKA position is about 20 Å below the loop center in the z direction. The final NPT relaxation is 40 ps instead of 20 ps to accommodate the higher PKA energy. Other simulation setup is similar to that for the smaller loop at 2 keV PKA energy. Regarding the PKA position, previous cascade overlapping simulations show that the final defect structures are very sensitive to the separation distance between the loop center and the PKA position [36]. In this work, we have examined about 400 snapshots at the thermal spike through visual inspection and found that in about 90% of simulations the cascades overlap completely with the pre-existing loop. Therefore, the choice of the PKA positions is reasonable. In addition, the PKA position is the same for a given PKA energy regardless of Cr concentration. Therefore, the effect of PKA position on the results (i.e., how the Cr concentration affects the <100> loop formation probability) can be excluded.

3. Results

3.1. Effect of Cr concentration on ½<111> to <100> transformation probability

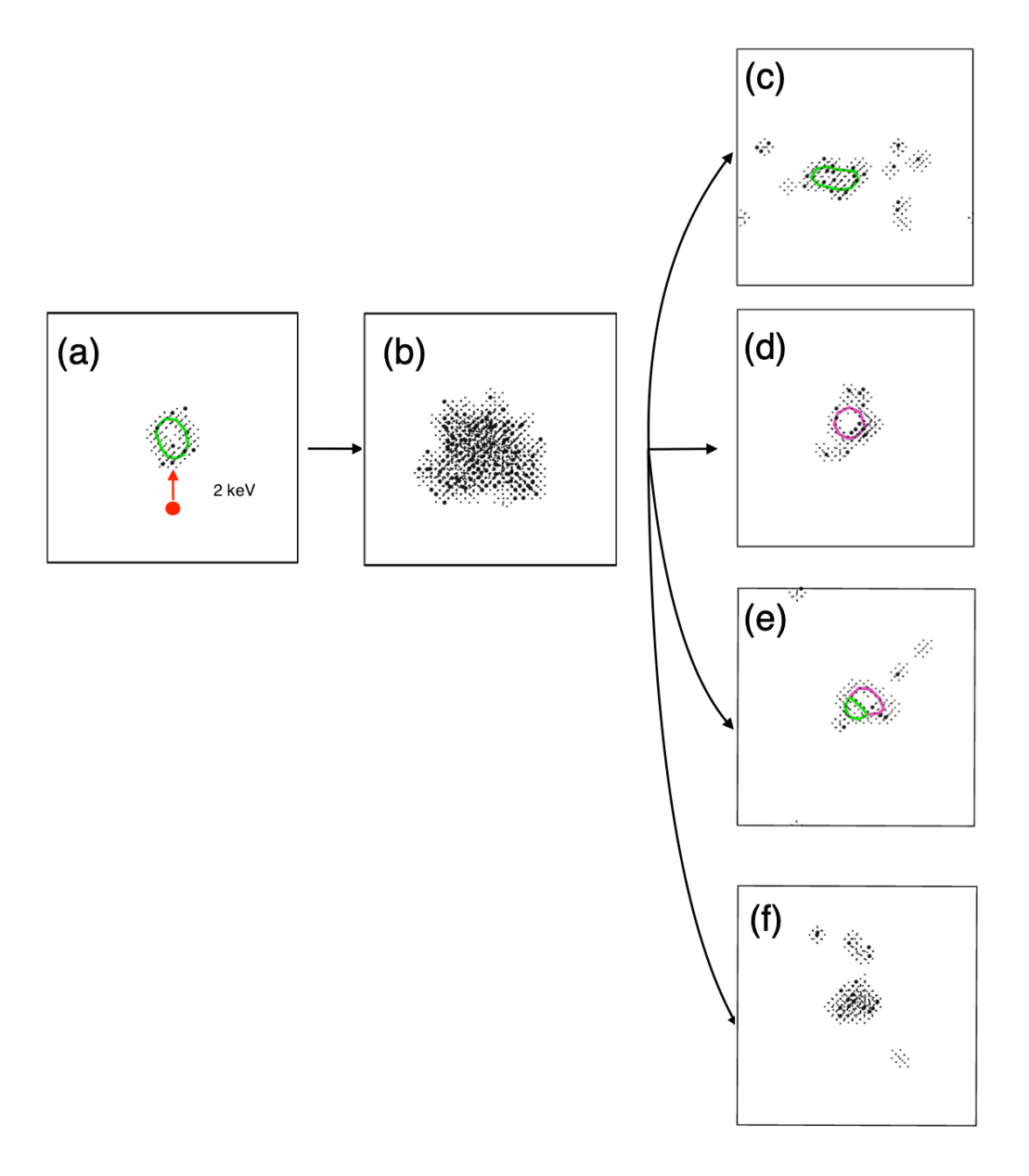


Figure 1. Representative snapshots from cascade overlapping simulations in an Fe-5%Cr alloy using the CD-EAM potential. Only non-BCC atoms are shown. (a) Initial configuration of a pre-existing ½<111> dislocation loop containing 35 interstitials. The red filled circle indicates the initial position of a PKA and the red arrow indicates its velocity direction. (b) Cascade overlapping with the pre-existing ½<111> loop during thermal spike. (c) Formation of a ½<111> loop. (d) Formation of a <100> loop. (e) Formation of a <100>+<111> mixed loop. (f) Formation of non-loop type interstitial clusters. Green lines: ½<111> loops/segments; purple lines: <100> loops/segments; Smaller black spheres: Fe atoms; Larger black spheres: Cr atoms.

Firstly cascade overlapping simulations are conducted on the smaller pre-existing \(\frac{1}{2} < 111 > \) loop (35 interstitials) with 2keV PKA energy using the CD-EAM potential. Figures 1(a-b) show that a PKA initiates a displacement cascade, which completely overlaps with the pre-existing ½<111> loop in an Fe-5%Cr alloy. After the cascade settles, a new defect structure can form. However, the new (final) defect structure is highly stochastic. Figures 1(c-f) show four representative final defect structures characterized by OVITO. In many simulations, the final defect structure still contains a ½<111> loop, although it can have a different geometry and Burgers vector direction from the initial one, as shown in Fig. 1(c). As expected, some isolated point defects can also form near the new loop. In some simulations, the pre-existing ½<111> loop transforms into a <100> loop (Fig. 1(d)). Note that the length of a new <100> loop is typically shorter than the original or a new ½<111> loop because the Burgers vector of a <100> loop is 15% larger than a $\frac{1}{2}$ <111> loop (i.e., a vs. $a\sqrt{3}/2$). If the total loop volume (V_{loop} , which is proportional to the number of interstitials) is conserved, the larger Burgers vector (b) leads to a smaller loop radius (r) based on the equation $V_{loop} = \pi r^2 \times b$. In a limited number of simulations, the final damage structures have a mixed loop structure consisting of both ½<111> and <100> loop segments, as shown in Fig. 1(e). In the rest of simulations neither type of dislocation loop forms, instead a large interstitial cluster forms (sometimes with a short loop segment), as shown in Fig. 1(f). All four types of defect structures have been found in both pure Fe and Fe-Cr alloys with Cr concentration ≤5%. When the Cr concentration is high (10% and 15%), mixed dislocation loops are not found.

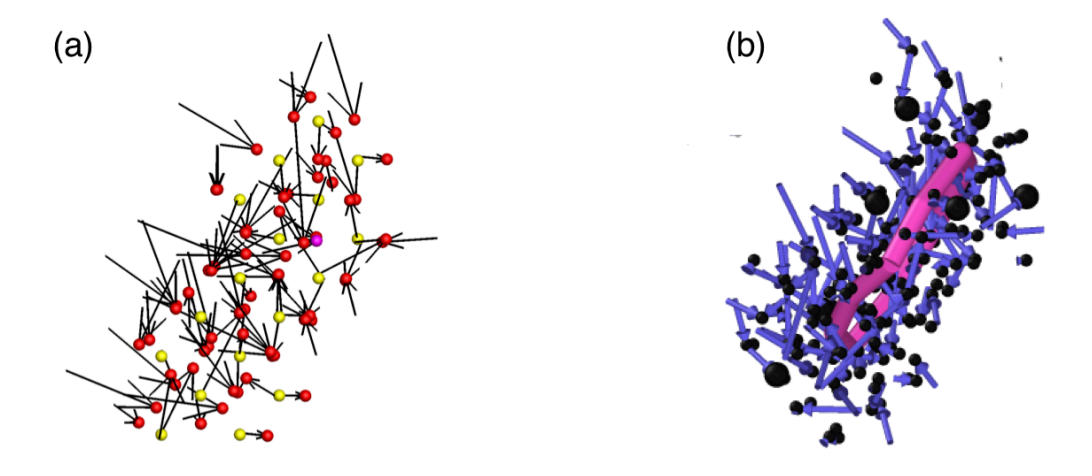


Figure 2. Vector plots of a final <100> loop structure in an Fe-5%Cr. The vector tails indicate the initial atom positions before the cascade is initiated and the heads show their current positions. (a) The loop structure characterized by the reference lattice site method. Here red and purple spheres are Fe and Cr interstitials, respectively. Yellow spheres are Fe vacancies. Cr vacancies are not observed in this snapshot. (b) The loop structure characterized by DXA in OVITO. Only non-BCC atoms are shown. Fe atoms and Cr atoms are shown as small and large black spheres, respectively. The <100> loop is illustrated by the thick purple line.

To investigate the ½<111> to <100> loop transformation mechanism in cascade overlapping simulations, Figure 2 shows two types of vector plots superimposing on a final <100> loop to illustrate where the atoms in the final loop come from. In Fig. 2(a), the <100> loop is characterized by the reference lattice site method [44, 56] in which the reference system is the perfect crystal that does not contain a loop. For each interstitial atom in the <100> loop, the vector tail indicates the initial position of the interstitial atom before overlapping cascade occurs and the vector head represents its current position. Clearly the vectors are randomly oriented, indicating that the formation of the <100> loop is not a direct rotation of the Burgers vector in the original ½<111> loop. Otherwise, the vectors would show a military-like coordinated motion and align along a certain direction. In Fig. 2(b), the <100> loop is characterized by the DXA method in OVITO. Similar to Fig. 2(a), the vector tails indicate where the original positions of the loop atoms before the cascade takes place. Again, the vectors are randomly oriented, further confirming that the displacement cascade does not change the Burgers vector of the pre-existing ½<111> loop through a military-like rotating/shearing process. In addition, the vectors in both Figs. 2(a) and 2(b) are short, indicating that atoms do not have longrange diffusion during the loop transformation. Therefore, the formation of a <100> loop as well as other defect structures shown in Fig. 1 should be a "re-precipitation" process. At the thermal spike (Fig. 1(b)), the loop atoms as well as their surrounding atoms are displaced from their original positions. However, different from cascade simulations in a single crystal in which equal numbers of interstitials and vacancies are created [13, 44, 50], the entire cascade is oversaturated with interstitials due to the breakup of a pre-existing interstitial loop. During the cascade recovery stage, the displaced atoms compete for the limited lattice sites. The atoms that are left behind form interstitials. These "precipitated' interstitials, which are not necessary to be the same interstitials as in the pre-existing $\frac{1}{2}$ <111> loop, rearrange themselves to form different types of defect structures, as shown in Figs. 1 (c) – (f). It should be noted that these results are based on the simulations in which a cascade can completely overlap with the pre-existing loop. If the cascade only overlaps partially with the loop, it is expected that the probability of loop transformation may be lower because the condition for interstitial re-precipitation is not satisfied. The extent of cascade overlapping can be related to the separation distance between the PKA position and the loop center, PKA energy, and the size of the pre-existing loop. In a recent cascade overlapping simulations in pure Fe by Byggmästar et al. [36], the authors have conducted systematic studies and found that the loop transformation probability is sensitive to these factors. Similar observations are also reported in the recent work by Wang et al. [20]. As mentioned in the Method Section, in this work the PKA positions are reasonably chosen because the majority of cascades can completely overlap with a pre-existing loop. Another remark is that in this re-precipitation mechanism, the pre-existing defect structure is not limited to a ½<111> loop. Other interstitial-rich structures, such as <100> loop and C15 clusters, can also be used as initial structures [20, 36] for cascade overlapping simulations because they can lead to oversaturated interstitials in a cascade. The final defect structures are expected to be similar as the ones shown in Fig. 1, although this expectation should be carefully verified in the future. If no such pre-existing interstitial-rich defect structures are present, a PKA typically creates a cascade structure having a vacancy-rich core and an interstitial-rich periphery. In such a case, direct nucleation of ½<111> or <100> interstitial loops at the interstitial-rich region is possible [13, 15], although the later may require a very high PKA energy [15].

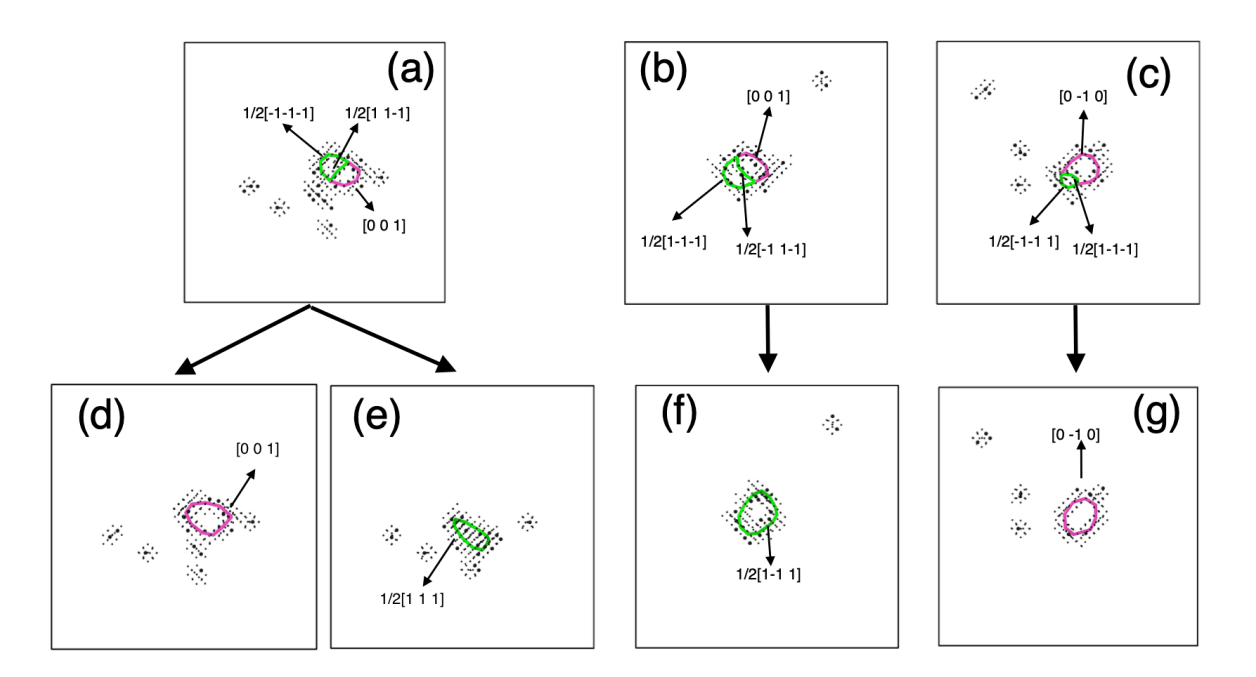


Figure 3. Evolution of mixed dislocation loops in the Fe-5%Cr alloy predicted by the CD-EAM potential. The upper panel shows three mixed loop structures produced from 2keV cascade overlapping simulations. The lower panel shows the predominant loop evolution results after 2 ns thermal annealing at 300 K. Green lines: ½<111> loops/segments; Purple lines: <100> loops/segments; Black arrows: Burgers vector directions. (a) Similar lengths of <100> and ½<111> loop segments. (b) Longer ½<111> loop segments than <100>; (c) Longer <100> loop segments than ½<111>. (d) A final <100> loop. (e) A final ½<111> loop. (f) A final ½<111> loop. (g) A final <100> loop.

The mixed dislocation loops produced from the cascade overlapping simulations may further evolve into a single loop through dislocation reaction during thermal annealing. It is found that the final annealed loop structure may depend on the relative length of the two types of loop segments in the initial mixed loop. Here some mixed loop structures produced from 2keV cascade overlapping simulations in the Fe-5%Cr alloy are selected for further thermal annealing simulations in an NPT ensemble for 0.2 ns at 300 K using the CD-EAM potential. These initial mixed loop structures are shown in Figs. 3(a-c). For each configuration, 20 independent annealing simulations are conducted. In Fig. 3(a), the mixed loop contains both <100> and $\frac{1}{2}$ <111> loop segments of similar lengths. Based on the DXA algorithm, the Burgers vectors of loop segments are $\frac{1}{2} \left[\overline{1} \ \overline{1} \ \overline{1} \right]$, $\frac{1}{2} \left[1 \ 1 \ \overline{1} \right]$, and $\left[0 \ 0 \ 1 \right]$. In some annealing simulations, the two $\frac{1}{2}$ <111> segments react with each other to form a <100> loop (Fig. 3(d)), through the following reaction based on conservation of Burgers vectors,

$$\frac{1}{2}[\overline{1}\overline{1}\overline{1}] + \frac{1}{2}[11\overline{1}] \rightarrow [00\overline{1}]. \tag{1}$$

Note here we treated $[0\ 0\ \overline{1}]$ and $[0\ 0\ 1]$ characterized by DXA as the same Burgers vector. In some other simulations, the reverse reaction of Eq. (1) occurs and the final loop is a ½<111> loop (Fig. 3(e)). Among the 20 annealing simulations using the configuration shown in Fig. 3(a), 10 of them evolve into a ½<111> loop and 8 of them evolve into a <100> loop, respectively. The rest 2 of them stay as a mixed loop. For the mixed loop shown in Fig. 3(b), the total length of <100> loop segment is about 9Å shorter than the total length of two ½<111> loop segments. In all 20 annealing simulations, the final loop is a ½<111> type, as shown in Fig. 3(f). The reaction is similar to Eq. (1), but in the reverse direction. For the third mixed loop configuration shown in Fig. 3(c), the total length of <100> loop segment is 11Å longer than the total length of $\frac{1}{2}<111>$ loop segments. In 20 annealing simulations, 14 of them form a <100> loop (Fig. 3(g)) and the rest of them form a ½<111> loop (not shown). The dislocation reaction, either in the forward or reverse direction, is also similar to Eq. (1). Based on the above analysis, it seems that the relative length difference between two types of loop segments may be an important factor for the evolution of mixed loops. If one type of loop segments has a predominant length, it can have a higher probability to evolve into a single loop of the same Burger vector. However, other factors such as the defects near the loop could also affect evolution of a mixed loop. The role of nearby defects on mixed loop evolution is not studied here because it is beyond the scope of this work.

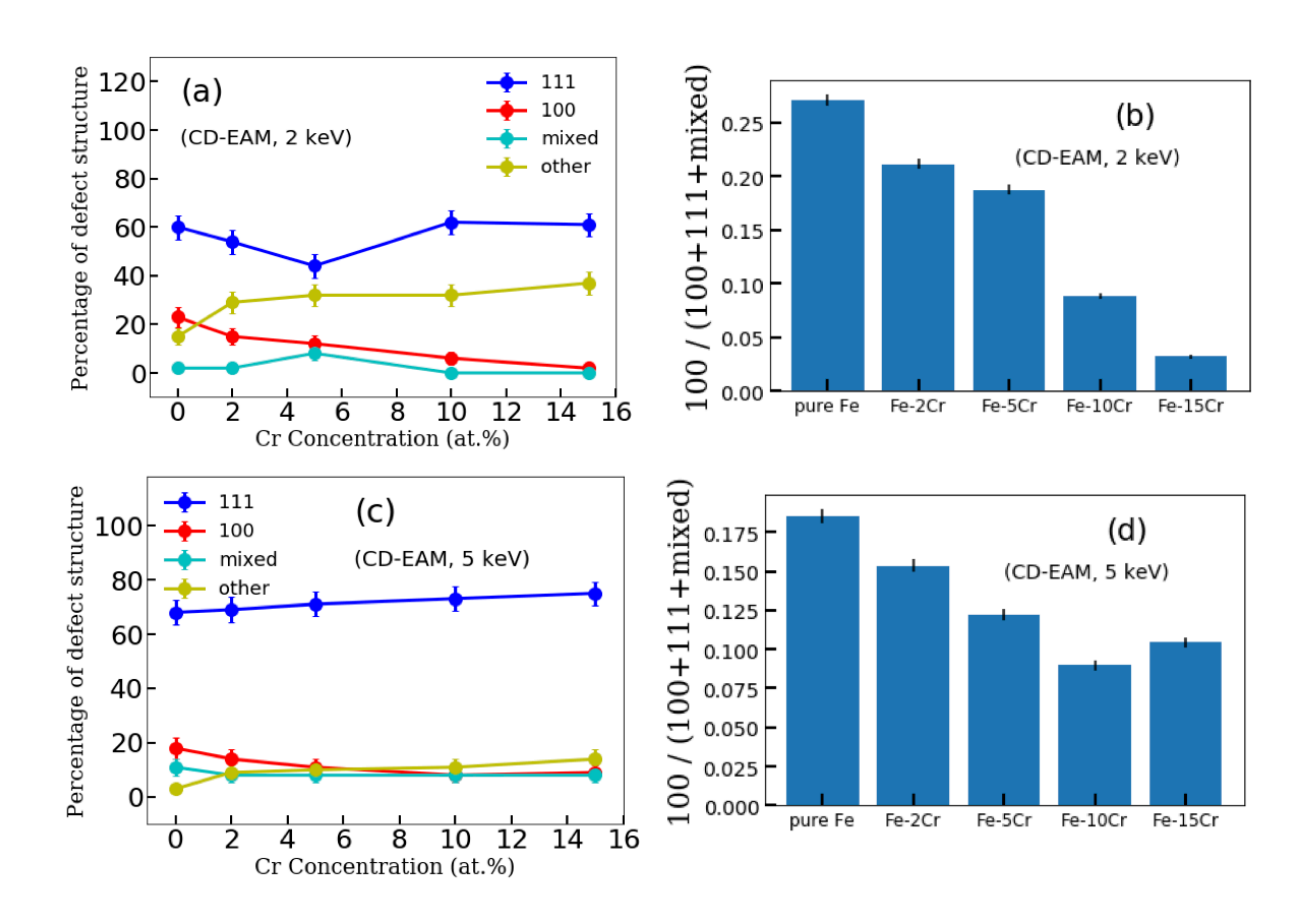


Figure 4. Statistics of different final defect structures at different Cr concentrations from cascade overlapping simulations on a pre-existing ½<111> dislocation loop at 300 K using the CD-EAM potential. (a) Percentages of different types of defect structures at different Cr concentrations for 2keV PKA energy on a 35-interstitial loop. (b) Fractions of <100> loops with respect to total loops (100 + 111 + mixed) in pure Fe and Fe-Cr alloys for 2keV PKA energy on a 35-interstitial loop. (c) Percentages of different types of defect structures at different Cr concentrations for 5keV PKA energy on a 55-interstitial loop. (d) Fractions of <100> loops with respect to total loops (100 + 111 + mixed) in pure Fe and Fe-Cr alloys for 5keV PKA energy on a 55-interstitial loop. In all plots, an error bar represents the confidence interval for a 95% of confidence level.

To study the effect of Cr concentration on the <100> loop formation probability, similar cascade overlapping simulations with a 2 keV PKA energy are conducted for pure Fe, Fe-2%Cr, Fe-5%Cr, Fe-10%Cr, and Fe-15%Cr systems using the CD-EAM potential. At each composition, statistics are based on 100 independent cascade simulations, as described in the Method Section. To have a fair comparison, all the final defect structures are obtained at 42 ps after a PKA is initiated. The percentages of the four types of final defect structures as a function of Cr concentration are shown in Fig. 4(a). Although the data fluctuate somewhat at 5% Cr, the overall trend is pretty clear. As the Cr concentration increases, the ½<111> loop formation probability remains at about 60% (except at 5% Cr). In contrast, the <100> loop formation probability decreases monotonically with the increasing Cr concentration, from about 23% in pure Fe to 2% in Fe-15%Cr. This trend clearly indicates that Cr suppresses the formation of <100> loops, which is consistent with many experimental observations [25, 26, 28, 31] discussed in the Introduction Section. For pure Fe, formation of a <100> loop is observed in about 23% of simulations, which is close to 18% in Wang et al.'s work [20] using the same Fe potential (M03) at 2keV energy at 300 K. Using other interatomic potentials for pure Fe, Wang et al. [20] predicted that the <100> loop formation probability is about 15% for the AM04 potential [57] and 32% for the M07 potential [58], respectively; Similarly, Byggmästar et al. [36] predicted that the <100> loop formation probability is about 10-20% at the full cascade overlap using the AM04, the original and modified M07 potentials [58, 59]. The formation probability of <111>+<100> mixed loops is very low at most of Cr concentrations, except in Fe-5%Cr. The reason is unclear and it could be induced by insignificant statistics. It should be noted that for the CD-EAM potential used in this work, the Fe-5%Cr has the most negative heating of mixing [44]. However, it is unclear if this is just a coincidence or the negative heating of mixing plays a role on the dislocation loop evolution.

As mentioned earlier, the <100> loop formation probability is also sensitive to many factors such as the separation distance between the PKA position and the loop center, PKA energy, and the size of the pre-existing loop [20, 36]. To explore these factors, cascade overlapping simulations are conducted using a larger pre-existing ½<111> loop containing 55 interstitials, a higher PKA energy of 5keV, a longer separation distance (~ 20 Å). The results are shown in Figs. 4(c). For pure Fe, the Fe component in the Bonny2011 potential is used, because the Fe components in both CD-EAM and Bonny2011 potentials are based on the same M03

potential. Again 100 simulations are performed at each Cr concentration. For ½<111> loops, the percentage increases slightly with Cr concentration. For <100> loops, the percentage decreases from around 20% to 10%. For mixed loops, the percentage is non-negligible. For other types of defect clusters, the percentage also increases slightly with Cr concentration, similar as in Fig. 4(a). Overall, the 5keV simulations also show that Cr can suppress the <100> loop formation, although the effect is not as significant as in the 2keV simulations (Fig. 4(a)).

For the other types of non-loop interstitial clusters, the probability increases slightly with the Cr concentration at both PKA energies, in particular from pure Fe to Fe-2%Cr. The presence of such interstitial clusters is reasonable because not all interstitial clusters can evolve into dislocation loops in experiments [26, 27, 32]. However, one may wonder if Cr causes a solute drag effect to slow down the recovery stage of cascades thus artificially suppresses the <100> loop formation. To explore this possible effect, five non-loop interstitial clusters from 2keV simulations in the Fe-10%Cr are randomly selected for an additional 0.2 ns annealing simulation at 300 K in a NPT ensemble. For each configuration, fifteen independent annealing simulations are conducted. Among these 75 annealing simulations, only in 7 simulations the defect structure transforms to a $\frac{1}{2}$ <111> loop and in 1 simulation the defect structure transforms to a <100> loop, while all others remain as the none-loop type of interstitial clusters. Therefore, the longer simulation time does not increase the formation probability of <100> loops, at least at the MD reachable timescale. The presence of other types of non-loop structures is also consistent with Béland et al.'s SEAKMC modeling [40] of reaction of two ½<111> loops in an Fe-10%Cr using a different interatomic potential, in which longer simulation times than MD could be achieved but still a substantial fraction of non-loop structures were observed.

In some experimental studies, the fraction of <100> or $\frac{1}{2}<111>$ loops out of total loops is reported [24, 31]. Here a similar approach is used for analyzing our modeling results. Figure 4(b) shows the fraction of <100> loops out of total loops (<100>, ½<111>, and mixed) in pure Fe and Fe-Cr alloys from 2keV simulations. It is clear that the <100> loop fraction decreases as Cr concentration increases, from about 27% in pure Fe to only about 3% in Fe-15%Cr. For 5keV simulations (Fig. 4(d)), the <100> loop fraction also decreases when the Cr concentration is up to 10%. At 15%, the fraction increases slightly, probably due to insignificant statistics. Overall, the trends in both 2keV and 5keV simulations are qualitatively consistent with Haley et al.'s experimental results [31]. In their work, the fraction of ½<111> loops out of total loops increases from about 50% to 85% (or equivalently the fraction of <100> loops decreases from 50% to 15%) as Cr concentration increases from 10% to 15% in Fe-Cr-Al alloys under Kr⁺⁺ irradiation at 320 °C, although the role of Al cannot be ruled out in their work. In our work, the only factor that affects the <100> loop fraction is Cr concentration for a given PKA energy. Therefore, we reasonably expect that Cr can indeed inhibit the <100> loop formation in Fe-Cr alloys. Note that in Béland et al.'s SEAKMC modeling [40] of the reaction of two ½<111> loops in pure Fe and Fe-10%Cr using a different potential, their results also indicate that the <100> loop formation probability in the Fe-10%Cr is slightly lower than in pure Fe (20% vs. 28%) when Cr is randomly distributed in the Fe matrix, although the statistical difference might be insignificant as the authors claimed.

3.2. Effects of Cr on defect energetics

Currently it is unclear why the increase of Cr content reduces the fraction of <100> dislocation loops in experiments. Some researchers [32, 60] interpreted this phenomenon based on the assumption that the reaction of \(\frac{1}{2} < 111 \right) \) dislocation loops (mechanism #2 discussed in the Introduction) is the dominant mechanism for <100> loop formation. They argued that some solute elements such as helium or Cr can reduce the loop mobility due to the solute drag effect and thus inhibit their encounter probability to form <100> loops. This explanation is certainly a reasonable argument. However, the <100> loop formation mechanism based on two gliding ½<111> loop reactions has been challenged [13, 15], because this mechanism requires that the two ½<111> loops should have similar sizes and overlapping gliding cylinders, which may not be easily satisfied in reality. In our previous MD simulations of defect production in Fe-based alloys [44, 50], we have demonstrated that defect formation energies such as Cr interstitial formation energy play a dominant role on the production fraction of Cr interstitials in Fe-Cr alloys during the primary damage stage. Following the same logic, here the formation energies of both ½<111> and <100> loops in Fe-Cr alloys of different Cr concentrations are calculated to determine if they have any correlation with the loop formation probabilities. The method for creating a ½<111> loop has been described in the Method Section. To create a <100> loop, a similar approach is used, but the habit plane is {100} and two extra layers of atoms are introduced as loop atoms [18]. After an energy minimization, a <100> loop can form. To have a fair comparison, the two types of loops have similar sizes – there are 35 and 37 interstitials in the ½<111> loop and <100> loop, respectively. Before creating a dislocation loop of either type, Cr atoms are randomly distributed in a pure Fe matrix according to its corresponding concentration. To get statistically meaningful results, 100 different configurations are created for each Cr concentration. Note that each loop also contains some randomly distributed Cr atoms and the Cr concentration in the loop is close to the average Cr concentration in the corresponding Fe-Cr alloy.

The formation energy of a dislocation loop per atom in an Fe-Cr or a pure Fe matrix is defined as,

$$E_f^{loop} = [E_{defect}^{loop} - E_{matrix} - (n - x) * \varepsilon_{Fe} - x * \varepsilon_{Cr}]/n, \tag{2}$$

 $E_f^{loop} = [E_{defect}^{loop} - E_{matrix} - (n - x) * \varepsilon_{Fe} - x * \varepsilon_{Cr}]/n, \tag{2}$ where E_{defect}^{loop} is the total energy of an Fe-Cr or pure Fe matrix containing a dislocation loop, E_{matrix} is the total energy of the perfect Fe-Cr or pure Fe matrix before a loop is introduced, ε_{Fe} is the cohesive energy per atom of a pure Fe, ε_{Cr} is the cohesive energy of a substitutional Cr in a pure Fe system, n is the number of total interstitials in a dislocation loop, and x is the number of Cr atoms in the loop. Note x is determined by the Cr concentration in the Fe-Cr alloys. Since in our calculations, 100 independent Fe-Cr configurations are used at each Cr concentration for each loop type, the loop formation energy has a distribution. Figures 5 (a) and 5(b) show the probability distribution functions (PDFs) of loop formation energy per atom at different Cr concentrations for both types of loops predicted by the CD-EAM potential. In Fig. 5(a), it can be seen that all the <100> loop formation energies (per atom) in the alloys are higher than that in the pure Fe (vertical dashed line). The peak value of each distribution shifts towards the highenergy side as the Cr concentration increases. For the $\frac{1}{2}$ <111> type loop (Fig. 5(b)), a similar trend can be found. However, the peak shift is not as significant as that for the <100> loop. For example, the peak value of the distribution for the <100> loop is at around 1.65 eV in the Fe-15%Cr while it is around 1.52 eV for the $\frac{1}{2}$ <111> loop. The results indicate that it becomes more and more difficult to form a <100> than a $\frac{1}{2}$ <111> loop as Cr concentration increases.

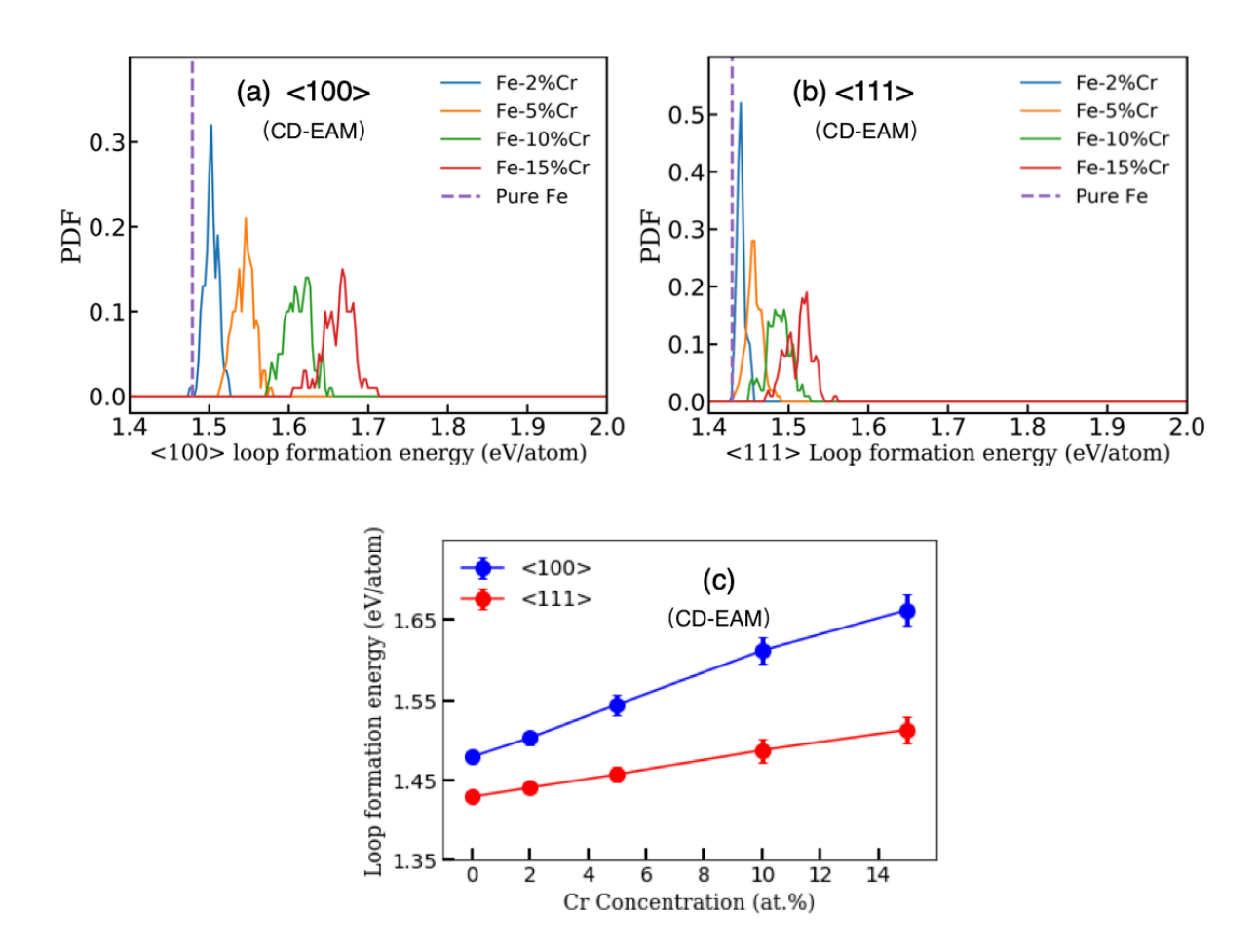


Figure 5. Effects of Cr concentration on the <100> and $\frac{1}{2}$ <111> loop formation energies in Fe-Cr alloys predicted by the CD-EAM potential. The <100> and $\frac{1}{2}$ <111> loops contain 37 and 35 interstitials, respectively. (a) Probability distribution functions (PDFs) of the <100> loop formation energy (per atom) at different Cr concentrations. (b) PDFs of the $\frac{1}{2}$ <111> loop formation energy at different Cr concentrations. (c) Average loop formation energies (per atom) of two loop types as a function of Cr concentration. The error bars represent standard deviations. Some error bars are smaller than the symbol size so they are invisible. Note that the <100> and $\frac{1}{2}$ <111> loop formation energies in the pure Fe are indicated by the purple dashed lines in (a) and (b), respectively.

To better illustrate how Cr concentration affects the dislocation loop formation energies, Figure 5(c) shows the *average* loop formation energies (per atom) for the <100> and ½<111> loops based on 100 independent configurations at each Cr concentration. The average loop formation energy increases with Cr concentration for both types of loops. However, the <100> loop increases at a much faster rate than the ½<111> loop, indicating that Cr influences the stability of <100> loops more strongly than that of ½<111> loops. In addition, at all Cr concentrations, the ½<111> loop has a lower average loop formation energy than the <100> loop. The relative stability between two types of loops explains why much more ½<111> loops than <100> loops are produced in our independent cascade overlapping simulations predicted by the CD-EAM potential (Fig. 4(a)). More importantly, our results show that the <100> loops become energetically less and less favorable than the ½<111> loops as Cr concentration increases, which is consistent with the decreasing fraction of <100> loops obtained in our cascade simulations (Fig. 4b) and previous experiments [25, 26, 28, 31]. In order to prove that the Cr effect is not specific to a certain loop size, similar calculations are conducted for <100> and ½<111> loops of about 20 interstitials. The results follow a similar trend as that shown in Fig. 5(c).

Figure 5 indicates that Cr atoms are energetically more favorable to stay in a ½<111> loop rather than a <100> loop. To understand the underlying reason, here the loop formation energies of <100> and ½<111> loops in a *pure* Cr are also calculated, using the same CD-EAM potential. The loop sizes are the same as the counterparts in pure Fe, which is about 36 interstitials in each type of loop. The loop formation energy per atom in pure Cr is 1.97 eV for the ½<111> loop and 2.48 eV for the <100> loop, in comparison to 1.43 eV for the ½<111> loop formation energy between a pure Fe and a pure Cr is 0.54 eV while that for the <100> loop is 1.0 eV. Therefore, Cr atoms are energetically more favorable to be incorporated in a ½<111> loop than a <100> loop in Fe-Cr alloys because the <100> loop formation energy in a pure Cr is much higher than that in a pure Fe. We think this could be the thermodynamic origin for why Cr suppresses the <100> loop formation probability in Fe-Cr alloys as predicted by the CD-EAM potential.

In Fig. 5, the dislocation loop formation energies are calculated based on the assumption that Cr atoms are randomly distributed in the Fe matrix as well as in the loops. However, Cr atoms may go to some preferred segregation sites in the loops if kinetics allows. Here the Cr segregation energies to both <100> and ½<111> loops in a pure Fe are calculated using the CD-EAM potential. A rectangular box that encloses a <100> or ½<111> loop is selected and only the atom sites within this box are used for segregation energy calculation. The box height, which is along the normal direction of the loop habit plane, is restricted to 20 Å to reduce the computational cost. The reference state for this calculation is a substitutional Cr in a bulk Fe. Therefore, a positive segregation energy indicates Cr segregation is unfavorable and vice versa. Figure 6 shows the segregation energy profiles for the two types of loops, in which the horizontal axis represents the distance in the radial direction from the loop center. For the segregation sites that are not on the loop plane, their positions are projected on the loop plane. Clearly, the magnitude of Cr segregation energy in the <100> loop is much larger than that in the $\frac{1}{2}$ <111> loop. Inside the <100> loop, the Cr segregation energy is positive. Inside the $\frac{1}{2}$ <111> loop, segregation energy can be either positive or negative. The results again indicate that it is more difficult to incorporate Cr atoms inside a <100> loop than a ½<111> loop. Near the loop edge, the Cr segregation energy in the <100> loop is more negative than that in the $\frac{1}{2}<111>$ loop. Therefore, segregation of sufficient number of Cr atoms into the loop edge may affect the relative stability of the two types of loops in Fe-Cr alloys. However, this situation may only happen when Cr atoms have sufficient kinetics at high temperatures. Moreover, in reality <100> loops may form before significant Cr segregation can take place at <100> loops, depending on the <100> loop formation mechanism. In this sense, it is reasonable to assume that Cr atoms are randomly distributed in our cascade overlapping simulations and loop formation energy calculations.

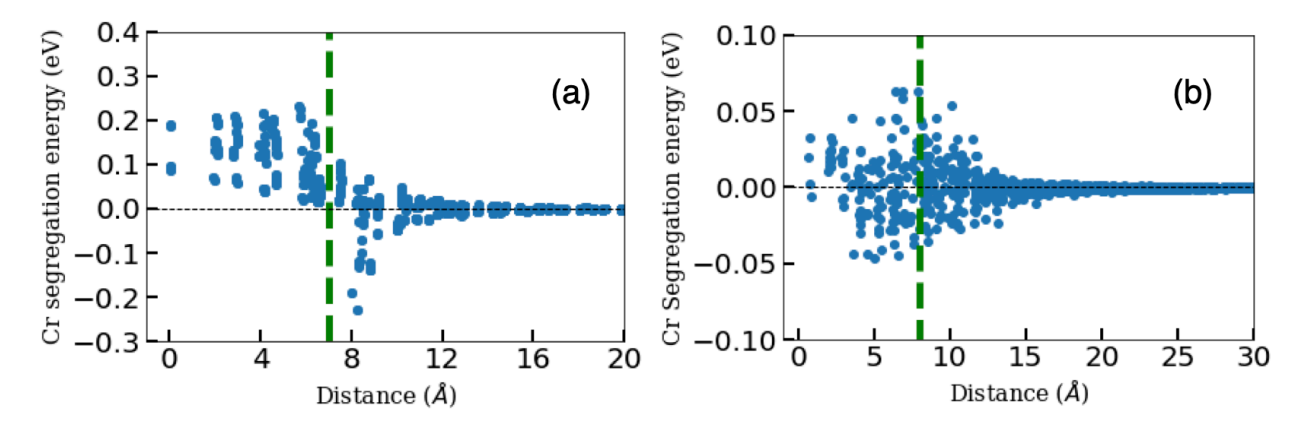


Figure 6. Cr segregation energy to (a) a <100> loop and (b) a ½<111> loop in a pure Fe. Each loop contains about 36 interstitials. The origin is at the loop center and the horizontal axis is the distance in the loop radial direction. The vertical green dashed line in each figure indicates the approximate loop edge position.

3.3. Effects of interatomic potentials

The results shown in Sections 3.1 and 3.2 are all based on the CD-EAM potential. In pure Fe, researchers have shown that the fraction of ½<111> to <100> loop transformation in cascade overlapping simulations depends on the choice of the interatomic potential [20, 36]. To check if our results are specific to the CD-EAM potential, the Bonny2011 2BM potential [49] is used to conduct some cascade overlapping simulations and loop formation energy calculations in a series of Fe-Cr alloys. The simulation conditions for the first set of cascade overlapping simulations are nearly identical to those simulations with 2 keV PKA energy using the CD-EAM potential, in which the pre-existing ½<111> loop contains 35 interstitials and the PKA is initiated at the same position. Again, at each Cr concentration, 100 independent cascade overlapping simulations are performed, and Cr atoms are randomly distributed in each simulation. The percentages of final defect structures are shown in Fig. 7(a). For the pure Fe, the distribution of different defect structures is very similar to that predicted by the CD-EAM potential (Fig. 4(a)). This is not surprising because the Fe components in both CD-EAM and Bonny2011 potentials are taken from the same M03 potential. As Cr concentration increases, the percentage of ½<111> loops remains around 60%, which is also similar to that predicted by the CD-EAM potential (Fig. 4(a)). However, the percentage of <100> loop fluctuates around 15-20% and does not show a substantial decrease as that predicted by CD-EAM (Fig. 4(a)). For mixed loops, the percentage is low, which is similar to that predicted by the CD-EAM. For other types of defect clusters, the

percentage is comparable to that for the <100> loops. Overall, although the Bonny2011 potential predicts some similar trends as the CD-EAM potential does, it does not predict that the <100> loop formation probability decreases significantly with the increasing Cr concentration, which is different from the results predicted by the CD-EAM potential (Fig. 4).

In addition to the 2keV energy simulations, 5keV cascade overlapping simulations are also conducted with a larger pre-existing ½<111> loop containing 55 interstitials using the Bonny2011 potential. The simulation conditions are similar to those in the 5keV simulations using the CD-EAM potential. The results are shown in Fig. 7(b). Again, 100 independent simulations are conducted at each Cr concentration and Cr atoms are randomly distributed in each simulation. For ½<111> loops, the percentage is still around 60%, which is similar to those at 2 keV PKA energy predicted by CD-EAM (Fig. 4(a)) and Bonny2011 (Fig. 7(a)) potentials. For <100> loops, the percentage is around 20% when the Cr concentration is up to 10%, which is similar to that at 2 keV PKA energy predicted by the Bonny2011 potential (Fig. 7a). At 15%Cr, the percentage of <100> loops drops somewhat. The percentage for mixed loops increases slightly with the Cr concentration while that for the other types of defects remains low. Overall, in both 2keV and 5keV simulations using the Bonny2011 potential, it seems that the formation probability of <100> loops is not sensitive to the Cr concentration.

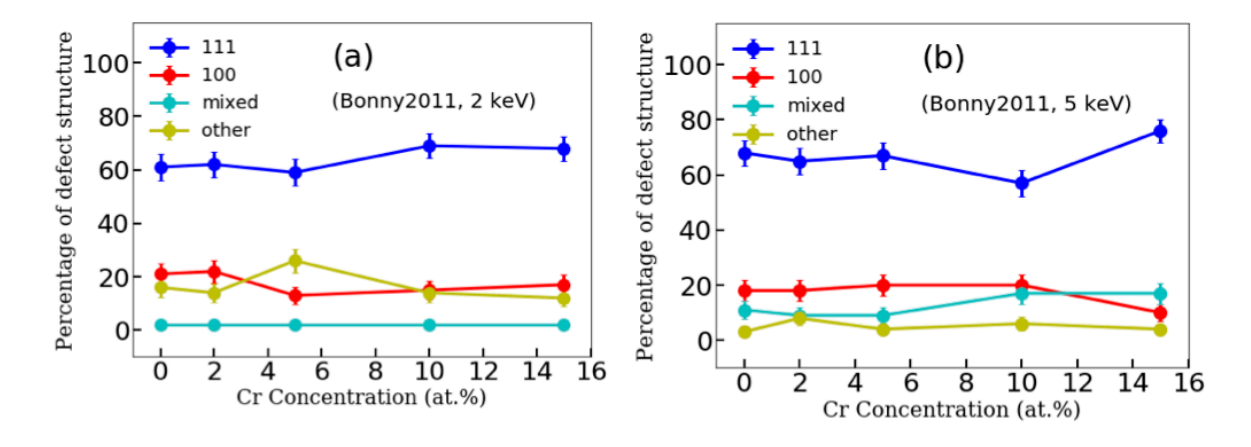


Figure 7. Statistics of the final defect structures at different Cr concentrations from cascade overlapping simulations on a pre-existing ½<111> dislocation loop at 300 K using the Bonny2011 2BM potential. (a) The ½<111> loop contains 35 interstitials and the PKA energy is 2 keV. (b) The ½<111> loop contains 55 interstitials and the PKA energy is 5 keV. In all plots, an error bar represents the confidence interval for a 95% of confidence level.

From Figs. 4 and 7, it can be clearly seen that the Cr effect on the <100> loop formation probability in Fe-Cr alloys depends on the choice of interatomic potential. Different potentials lead to different conclusions: The CD-EAM potential predicts that Cr suppresses the formation of <100> loops, which is consistent with many experimental observations; In contrast, the Bonny2011 potential predicts that Cr has a weak effect on the <100> loop formation probability. To understand why the Bonny2011 potential predicts such an effect, molecular statics calculations are conducted to calculate the <100> and $\frac{1}{2}<111>$ loop formation energies at

different Cr concentrations in Fe-Cr alloys, using a similar approach described in Section 3.2. Again, the <100> and ½<111> loops contain 37 and 35 interstitials, respectively; At each Cr concentration, 100 randomly distributed Cr configurations are used to ensure a good statistics. The average loop formation energies as a function of Cr concentration are shown in Fig. 8. Similar to those predicted by the CD-EAM potential (Fig. 5(c)), both loop formation energies increase with the increasing Cr concentration. In addition, the <100> loop always has a higher formation energy than the ½<111> loop, which is consistent with the independent cascade overlapping results that more ½<111> loops than <100> loops form (Fig. 7). However, different from Fig. 5(c) in which the <100> loop formation energy has a faster increase rate than that of ½<111> loop, the Bonny2011 potential predicts that both loops have nearly the same increase rate with the increasing Cr concentration, although the <100> loop has a slightly faster increase rate, as shown in Fig. 8. In other words, the Bonny2011 potential predicts that the relative stability between <100> and ½<111> loops does not change much as Cr concentration increases. This is likely to be the underlying reason why the formation probability of ½<111> loops remains around 60% while that of the <100> loops remains at about 20% at most of Cr concentrations as predicted by the Bonny2011 potential (Fig. 7).

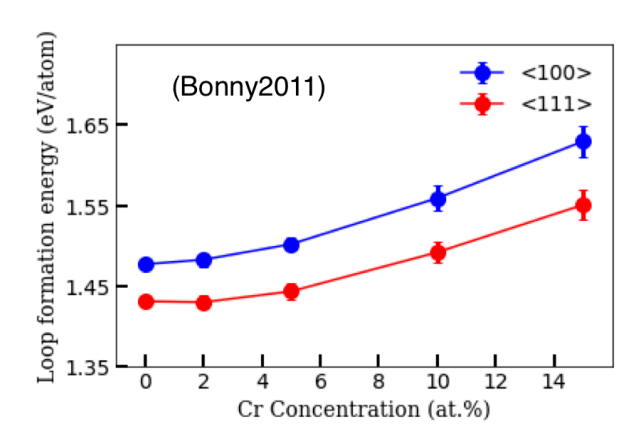


Figure 8. Average loop formation energies (per atom) of two loop types as a function of Cr concentration predicted by the Bonny2011 2BM potential. The <100> and $\frac{1}{2}<111>$ loops contain 37 and 35 interstitials, respectively. The error bars represent standard deviations. Some error bars are smaller than the symbol size so they are invisible.

Since the two potentials predict different trends in the effect of Cr on <100> loop formation probability, one may wonder which potential predicts a more reasonable trend on this subject matter. In both potentials, the Fe components come from the same M03 potential. In addition, both potentials also predict reasonable heat of mixing curves. Therefore, here the defect properties of pure Cr predicted by the two potentials are compared. The results are listed in Table 1 along with the available density functional theory (DFT) results reported in literature [46, 47]. The CD-EAM potential predicts very similar <100> and <111> self-interstitial-atom (SIA) formation energies of pure Cr as in DFT, while the Bonny2011 potential underestimates these energies. More importantly, the energy difference between <100> and <111> SIAs in pure Cr is

1.22 eV for CD-EAM but only 0.50 eV for Bonny2011, while DFT predicts the difference is 0.93 – 1.10 eV. This means that changing Cr interstitials from <111> to <100> is energetically more unfavorable in CD-EAM than in Bonny2011. For the difference in formation energy between <100> and ½<111> loops, the CD-EAM potential also predicts a higher energy difference than the Bonny2011 potential does (0.51 vs. 0.36 eV/atom). However, there is no DFT data available to determine which potential predicts more reasonable loop formation energies to our best of knowledge. These defect properties in pure Cr, together with the Cr concentration-dependent loop formation energies shown in Fig. 5(c) and Fig. 8, can help us explain why the two potentials predict different trends regarding the Cr effect on <100> loop formation probability. Since the CD-EAM potential predicts similar Cr point defect energetics as DFT, and most importantly it predicts a consistent trend with many experimental observations in terms of Cr effect on <100> loop formation probability [25, 26, 28, 31], we think that the CD-EAM potential predicts a more reasonable trend for this specific subject matter based on the currently available data, although this conclusion is not decisive.

Table 1. Comparison of self-interstitial-atom (SIA) and dislocation loop formation energies in pure Cr predicted by the CD-EAM and Bonny2011 2BM potentials. The <100> and ½<111> loops contain 37 and 35 interstitials, respectively. All energies are in the unit of eV for SIAs and eV/atom for loops.

Formation energy in	CD-EAM	Bonny2011	DFT
pure Cr			
$E_{SIA}^{<100>}$	6.83	4.55	6.78 [47]
$E_{SIA}^{<111>}$	5.62	4.05	5.68 [47]
$E_{SIA}^{<100>} - E_{SIA}^{<111>}$	1.21	0.50	0.93 [46], 1.10 [47]
$E_{loop}^{<100>}$	2.48	2.09	
$E_{loop}^{<111>}$	1.97	1.73	
$E_{loop}^{<100>} - E_{loop}^{<111>}$	0.51	0.36	

3.4. Prediction of effects of other BCC alloying elements on <100> loop formation

In Fig. 5, our molecular statics results using the CD-EAM potential show that adding Cr into Fe leads to a faster increase rate in loop formation energy for <100> than ½<111> loops. The defect energetics provide a reasonable explanation for why Cr suppresses the formation of <100> loops observed in our independent cascade overlapping simulations using this potential as well as in many previous experiments. On the other hand, the Bonny2011 potential predicts that the <100> loop formation probability is insensitive to Cr concentration, because this potential predicts that the Cr addition leads to similar increase rates in the <100> and ½<111> loop formation energies. The results from two different potentials also demonstrate that the cascade overlapping results have a strong correlation with defect/loop formation energies. In Table 1, we also showed that the formation energy differences between <100> and <111> types of defects in pure Cr can be correlated with the effect of Cr on <100> loop formation probability. This because it is energetically unfavorable for Cr to form interstitial-type defect structures with a <100> type Burgers vector with respect to the <111> type. Similarly, we may use the difference

between <100> and <111> SIA and loop formation energies in pure metals as a criterion to predict if other BCC alloying elements also have a similar effect as Cr. Here the formation energies of the SIAs and loops of <100> and <111> types in a few other BCC metals are calculated using empirical potentials, including tungsten (W) [61], vanadium (V) [62], molybdenum (Mo) [63], niobium (Nb) [64], and tantalum (Ta) [65]. The number of interstitials in each type of loop is also around 36. The results are shown in Table 2, along with those for pure Fe and Cr calculated using the CD-EAM potential. In addition, the differences in formation energy between <100> and <111> SIA dumbbells in these pure metals reported in literature [46], which were obtained by the DFT calculations, are also shown for comparison. For the energy difference between <100> and <111> SIAs, the results predicted by empirical potentials have some discrepancies with DFT results. Therefore, the following discussion is based on the SIA energy differences predicted by DFT and loop energy differences predicted by empirical potentials.

For loops in pure Fe, the difference in the formation energy per atom between two types of loops is very small (0.05 eV) and the ½<111> loop is slightly more favorable. For all other elements, the <100> loop has a non-negligible higher energy than the $\frac{1}{2}<111>$ loop. Therefore, if these elements are added to BCC Fe as alloying elements, they may reduce the formation probability of <100> loops, as Cr does. However, they may suppress the <100> loop formation probability differently. For Nb and W, the difference between two types of loops is small, about 0.11 eV and 0.10 eV, respectively. Therefore, they may only suppress the <100> loop formation slightly with respect to pure Fe. In Ta and Mo, the energy difference is moderate, about 0.37 eV and 0.45 eV, respectively. As a result, they may suppress the <100> loop formation moderately. For Cr and V, the energy difference is high, about 0.51 eV and 0.58 eV, respectively. In turn, they may have the strongest effect on inhibiting the <100> loop formation. Therefore, based on the difference in loop formation energies predicted by empirical potentials, the effect of suppressing <100> loop formation should follow the order: Fe < W \sqcap Nb < Ta < Mo < Cr < V. On the other hand, if we use the DFT results of the energy difference between <100> and <111> SIA dumbbells [46] as a criterion, the order is: Fe < V < Nb < Cr < Ta < Mo < W. The major discrepancies are for W and V, which have opposite trends predicted by the two criteria. Regardless which criterion to use, it seems that Nb will have a relatively weak effect while Mo and Cr will have a relatively strong effect. However, it should be emphasized that this conclusion is just a speculation. Currently there is no available experimental evidence to support this prediction. Therefore, future systematic studies or target experiments may be conducted to prove or disapprove this hypothesis.

Table 2. Formation energies of <100> ($E_{SIA}^{<100>}$) and <111> ($E_{SIA}^{<111>}$) SIA dumbbells as well as the formation energies per atom of <100> ($E_{loop}^{<100>}$) and $\frac{1}{2}<111>$ ($E_{loop}^{<111>}$) loops in pure BCC metals predicted by empirical potentials. Each type of loop contains about 36 interstitials. The energy difference between <100> and <111> SIA dumbbells predicted by DFT [46] are also shown for comparison. All energies are in the unit of eV for SIAs and eV/atom for loops.

	Fe	Cr	W	V	Mo	Nb	Ta
$E_{SIA}^{<100>}$	4.34	6.83	9.79	3.21	6.65	4.61	5.33
$E_{SIA}^{<111>}$	4.01	5.62	8.89	2.81	5.72	4.22	4.46

$E_{SIA}^{<100>}$ - $E_{SIA}^{<111>}$ (EAM, this work)	0.33	1.21	0.90	0.4	0.93	0.39	0.87
$E_{SIA}^{<100>}$ - $E_{SIA}^{<111>}$ (DFT [46])	0.30	0.96	1.94	0.55	1.59	0.70	1.17
$E_{loop}^{<100>}$	1.48	2.48	3.35	1.61	2.85	2.05	2.22
$E_{loop}^{<111>}$	1.43	1.97	3.25	1.03	2.40	1.94	1.85
$E_{loop}^{<100>}$ - $E_{loop}^{<111>}$ (EAM, this work)	0.05	0.51	0.10	0.58	0.45	0.11	0.37

4. Discussion and Conclusions

In this work, molecular dynamics simulations are firstly conducted to study how Cr concentration affects the formation probability of <100> interstitial-type dislocation loops in Fe-Cr alloys, using the concentration-dependent EAM (CD-EAM) potential [42]. The Cr concentration ranges from 0% (pure Fe) to 15%. The simulations for ½<111> to <100> loop transformation are based on the method of cascade overlapping on a pre-existing ½<111> dislocation loop at 300 K. The defect structures obtained from the cascade overlapping simulations include ½<111> loops, <100> loops, mixed loops, and non-loop interstitial clusters. The statistics is based on 100 independent simulations at each Cr concentration. The results show that the fraction of ½<111> loops among all the final defect structures remains nearly constant (~60%) while that of <100> loops decreases monotonically as the Cr concentration increases. The results clearly demonstrate that the formation probability of <100> loops decreases with the increasing Cr content in Fe-Cr alloys as predicted by this CD-EAM potential. The trend is consistent with many experimental observations [25, 26, 28, 31], although some other experiments reported contradictory results [32-34]. It is likely that the experimental results may be affected by many factors such as irradiation conditions, characterization techniques, and the presence of other alloying elements. In contrast, all our cascade overlapping simulations are conducted at nearly identical conditions except for the Cr concentration for a given PKA energy, which ensures a fair comparison and minimizes the factors that may affect the results. It should be emphasized that although the cascade overlapping method is used as a convenient way to demonstrate this Cr effect, the physical origin of Cr effect on <100> loop formation (i.e., due to defect energetics as discussed below) is not constrained to this method. This means that the Cr effect on <100> loop formation can be applied to other scenarios including electron irradiation in which cascade overlapping does not occur.

To explore the underlying origin for why Cr suppresses the formation of <100> loops more strongly than $\frac{1}{2}$ <111> loops as predicted by the CD-EAM potential, the probability distribution functions (PDFs) of both <100> and $\frac{1}{2}$ <111> loops are calculated by independent molecular statics calculations, based on 100 different configurations at each Cr concentration. The results show that the PDFs of both loop types shift to higher loop formation energy side as Cr concentration increases, but the magnitude of the shift for <100> loops is much larger than for $\frac{1}{2}$ <111> loops. Similarly, the average loop formation energy of the <100> loop type has a much faster increase rate than that of the $\frac{1}{2}$ <111> loop type as Cr concentration increases. The results demonstrate that the increasing Cr concentration causes <100> loops more and more difficult to

form than ½<111> loops from an energetic point of view. The results are consistent with our independent cascade overlapping simulations in which the fraction of ½<111> loops remains nearly constant while that of <100> loops decreases substantially with the increasing Cr content. Our further analysis shows that the difference in the formation energy between <100> and <111> SIAs/loops in pure Cr is much larger than that in pure Fe, which is consistent with previous DFT calculations that a <100> SIA dumbbell has a much higher formation energy than a <111> SIA dumbbell in pure Cr. In turn, it is energetically less favorable for Cr atoms to stay in a <100> loop than in a ½<111> loop in Fe-Cr alloys. In the previous kinetics-based explanation, Cr reduces the mobility of ½<111> loops and thus inhibits the reaction of two ½<111> loops to form a <100> loop [32, 60]. This kinetics-based explanation is certainly a plausible mechanism, although the limitation is that the two ½<111> loops should have similar sizes and overlapping gliding cylinders. In our explanation that is based on how Cr influences the relative stability of two loop types, such a restriction is not necessary. Actually, regardless of which of the aforementioned six <100> loop formation mechanisms is predominant, our explanation can be applied to interpret the Cr effect on inhibiting <100> loop formation, because the relative abundance of the two loop types correlates with their relative stability as this work shows. The two mechanisms do not contradict each other and they may operate concurrently. Therefore, our explanation can be considered as another possible mechanism in addition to the kinetics-based mechanism to explain the Cr effects on <100> loop formation probability.

To check if above conclusions are sensitive to the choice of interatomic potentials, the Bonny2011 2BM potential [49] is used to repeat the cascade overlapping simulations. Interestingly, this potential predicts that ½<111> and <100> loop formation probabilities remain around 60% and 20% for most Cr concentrations. In other words, this potential predicts that the <100> loop formation probability is not sensitive to the Cr concentration, which contradicts the results predicted by the CD-EAM potential. Our further molecular statics calculations reveal that this potential predicts similar increase rates of the <100> and ½<111> loop formation energies with the increasing Cr concentration. As a result, the relative stability between the two loop types does not change much with the increasing Cr concentration, explaining why this potential predicts that the <100> loop formation probability is not sensitive to Cr concentration. We compared the relevant point defect energetics of pure Cr predicted by the two potentials against the DFT results in literature and found that the CD-EAM potential predicts more reasonable defect energetics in pure Cr than the Bonny2011 potential does. In addition, given the fact that the CD-EAM potential predicts a consistent trend with many experimental observations in terms of the Cr effect on <100> loop formation probability in Fe-Cr based alloys, it is reasonable to believe that the results predicted by the CD-EAM potential are more physically sound.

Similar to the argument for Cr alloying element, the possible effects of other BCC alloying elements (Nb, V, Ta, Mo, W) on the <100> loop formation probability are also predicted based on the SIA and loop formation energies in pure metals. Our analysis suggests that all these alloying elements may suppress the <100> loop formation in Fe-based alloys, although Nb may have a relatively weak effect while Mo and Cr may have relatively strong effects. Currently no direct experimental evidence can be found to support this prediction due to the lack of systematic studies related to the effects of different alloying elements on dislocation loop evolution in Fe-based ferritic alloys. However, this work may motivate the research community to design target experiments or conduct modeling studies to prove or disapprove our predictions in the future. For non-BCC alloying elements or impurities, no analysis has been conducted as it is beyond the scope of this work, but it could be a good research topic in the

future. In particular, carbon (C) is a commonly used alloying element in Fe-based steels. Different from many other alloying elements that are mainly substitutional elements, carbon atoms can stay at the interstitial sites. In an early electron irradiation experiment on Fe-Cr alloys containing carbon impurities [66], the results indicated that carbon might suppress the formation of ½<111> loops but not <100> loops. However, some recent studies showed that other interstitial-type impurities such as silicon [67] and helium [32] may suppress the formation of <100> loop type more strongly than ½<111> type in FeCr-based alloys. Therefore, the effect of carbon on the dislocation loop formation may be very complex, which deserves dedicated experimental and computational studies in the future.

As mentioned in the Results Section, the <100> loop formation probability in cascade overlapping simulations can be affected by many factors such as PKA position, PKA energy, PKA direction, the size of the pre-existing loop, interatomic potential, etc. [20, 36]. In addition, the <100> loop formation probability may also depend on the structures of the pre-existing interstitial clusters (e.g., ½<111> loops, C15 clusters, <100> loops) [20, 36]. Therefore, there is a large parameter space to be explored in the future in order to have a more comprehensive understanding on how Cr or other alloying elements influence the <100> loop formation in Febased alloys. A final remark is that in reality <100> loops can become more stable than ½<111> loops at high temperatures in pure Fe and Fe-Cr alloys. In pure Fe, the transition temperature is found at around 400 °C under self-ion irradiation [24]. As mentioned earlier, the potentials used in this work cannot predict such a temperature dependence on the relative stability between two loop types. Therefore, the conclusions from this work should be only applied to the temperature range below the ½<111> to <100> transition temperature. On the other hand, our work suggests that the addition of Cr (and possibly other alloying elements as well) will increase the ½<111> to <100> transition temperature in Fe-Cr alloys with respective to pure Fe because Cr influences the relative stability between two loop types. This prediction could be validated by systematic studies of the combined temperature and composition effects on dislocation loop evolution in irradiated FeCr-based alloys in the future.

Acknowledgements

This material is based upon work supported by the National Science Foundation under Grant No. 1847780. X.M. B. also acknowledges Virginia Tech startup fund for partially supporting this work. The authors acknowledge the Advanced Research Computing at Virginia Tech for providing the high performance computing resources to this work.

Data availability statement

The raw/processed data required to reproduce these findings cannot be shared at this time due to technical or time limitations.

References

- [1] S.J. Zinkle, J.T. Busby, Structural materials for fission & fusion energy, Mater Today 12(11) (2009) 12-19.
- [2] R.L. Klueh, A.T. Nelson, Ferritic/martensitic steels for next-generation reactors, J Nucl Mater 371(1-3) (2007) 37-52.
- [3] E.A. Little, D.A. Stow, Void-Swelling in Irons and Ferritic Steels .2. Experimental Survey of Materials Irradiated in a Fast-Reactor, J Nucl Mater 87(1) (1979) 25-39.
- [4] F. Garner, M. Toloczko, B. Sencer, Comparison of swelling and irradiation creep behavior of fcc-austenitic and bcc-ferritic/martensitic alloys at high neutron exposure, J Nucl Mater 276(1-3) (2000) 123-142.
- [5] A.M.D. S.I. Porollo, A.N. Vorobeev, The microstructure and tensile properties of Fe–Cr alloys after neutron irradiation at 400 °C to 5.5–7.1 dpa, J. Nucl. Mater. 256 (1998) 247-253.
- [6] A. Aitkaliyeva, L. He, H. Wen, B. Miller, X.-M. Bai, T. Allen, Irradiation effects in Generation IV nuclear reactor materials, Structural Materials for Generation IV Nuclear Reactors, Elsevier2017, pp. 253-283.
- [7] G.S. Was, J.P. Wharry, B. Frisbie, B.D. Wirth, D. Morgan, J.D. Tucker, T.R. Allen, Assessment of radiation-induced segregation mechanisms in austenitic and ferritic-martensitic alloys, J Nucl Mater 411(1-3) (2011) 41-50.
- [8] M. Bachhav, G.R. Odette, E.A. Marquis, Microstructural changes in a neutron-irradiated Fe-15 at.%Cr alloy, J Nucl Mater 454(1-3) (2014) 381-386.
- [9] M. Bachhav, G.R. Odette, E.A. Marquis, alpha 'precipitation in neutron-irradiated Fe-Cr alloys, Scripta Mater 74 (2014) 48-51.
- [10] D. Terentyev, D.J. Bacon, Y.N. Osetsky, Reactions between a 1/2(111) screw dislocation and (100) interstitial dislocation loops in alpha-iron modelled at atomic scale, Philos Mag 90(7-8) (2010) 1019-1033.
- [11] A. Lehtinen, L. Laurson, F. Granberg, K. Nordlund, M.J. Alava, Effects of precipitates and dislocation loops on the yield stress of irradiated iron, Scientific reports 8(1) (2018) 6914.
- [12] A. Lehtinen, F. Granberg, L. Laurson, K. Nordlund, M.J. Alava, Multiscale modeling of dislocation-precipitate interactions in Fe: From molecular dynamics to discrete dislocations, Physical Review E 93(1) (2016) 013309.
- [13] Y. Zhang, D. Schwen, Y. Zhang, X.-M. Bai, Effects of oversized tungsten on the primary damage behavior in Fe-W alloys, Journal of Alloys and Compounds 794 (2019) 482-490.
- [14] R.E. Stoller, Primary Radiation Damage Formation, Comprehensive Nuclear Materials, Vol 1: Basic Aspects of Radiation Effects in Solids/Basic Aspects of Multi-Scale Modeling (2012) 293-332.
- [15] Q. Peng, F. Meng, Y. Yang, C. Lu, H. Deng, L. Wang, S. De, F. Gao, Shockwave generates< 100> dislocation loops in bcc iron, Nature communications 9(1) (2018) 4880.
- [16] A. Chartier, M.-C. Marinica, Rearrangement of interstitial defects in alpha-Fe under extreme condition, Acta Materialia 180 (2019) 141-148.

- [17] B. Eyre, R. Bullough, On the formation of interstitial loops in bcc metals, Philos Mag 12(115) (1965) 31-39.
- [18] J. Marian, B.D. Wirth, J.M. Perlado, Mechanism of formation and growth of < 100 > interstitial loops in ferritic materials, Phys Rev Lett 88(25) (2002) 255507.
- [19] H. Xu, R.E. Stoller, Y.N. Osetsky, D. Terentyev, Solving the puzzle of (100) interstitial loop formation in bcc iron, Phys Rev Lett 110(26) (2013) 265503.
- [20] X. Wang, N. Gao, Y. Wang, H. Liu, G. Shu, C. Li, B. Xu, W. Liu, Molecular dynamics study on the Burgers vector transition of nanometric dislocation loops induced by cascade in bcciron, J Nucl Mater 519 (2019) 322-331.
- [21] J. Chen, N. Gao, P. Jung, T. Sauvage, A new mechanism of loop formation and transformation in bcc iron without dislocation reaction, J Nucl Mater 441(1-3) (2013) 216-221.
- [22] Y. Zhang, X.-M. Bai, M.R. Tonks, S.B. Biner, Formation of prismatic loops from C15 Laves phase interstitial clusters in body-centered cubic iron, Scripta Mater 98 (2015) 5-8.
- [23] F. Granberg, J. Byggmästar, A. Sand, K. Nordlund, Cascade debris overlap mechanism of 100> dislocation loop formation in Fe and FeCr, Europhys. Lett 119(5) (2017).
- [24] Z. Yao, M. Jenkins, M. Hernández-Mayoral, M. Kirk, The temperature dependence of heavy-ion damage in iron: A microstructural transition at elevated temperatures, Philos Mag 90(35-36) (2010) 4623-4634.
- [25] M. Matijasevic, W. Van Renterghem, A. Almazouzi, Characterization of irradiated single crystals of Fe and Fe–15Cr, Acta Materialia 57(5) (2009) 1577-1585.
- [26] S. Porollo, A. Dvoriashin, A. Vorobyev, Y.V. Konobeev, The microstructure and tensile properties of Fe–Cr alloys after neutron irradiation at 400 C to 5.5–7.1 dpa, J Nucl Mater 256(2-3) (1998) 247-253.
- [27] M. Jenkins, Z. Yao, M. Hernández-Mayoral, M. Kirk, Dynamic observations of heavy-ion damage in Fe and Fe–Cr alloys, J Nucl Mater 389(2) (2009) 197-202.
- [28] D. Gelles, Microstructural examination of neutron-irradiated simple ferritic alloys, J Nucl Mater 108 (1982) 515-526.
- [29] K. Arakawa, K. Ono, M. Isshiki, K. Mimura, M. Uchikoshi, H. Mori, Observation of the one-dimensional diffusion of nanometer-sized dislocation loops, Science 318(5852) (2007) 956-959.
- [30] S. Dudarev, R. Bullough, P. Derlet, Effect of the α γ phase transition on the stability of dislocation loops in bcc iron, Phys Rev Lett 100(13) (2008) 135503.
- [31] J.C. Haley, S.A. Briggs, P.D. Edmondson, K. Sridharan, S.G. Roberts, S. Lozano-Perez, K.G. Field, Dislocation loop evolution during in-situ ion irradiation of model FeCrAl alloys, Acta Materialia 136 (2017) 390-401.
- [32] A. Prokhodtseva, B. Décamps, A. Ramar, R. Schäublin, Impact of He and Cr on defect accumulation in ion-irradiated ultrahigh-purity Fe (Cr) alloys, Acta Materialia 61(18) (2013) 6958-6971.

- [33] S. Xu, Z. Yao, M. Jenkins, TEM characterisation of heavy-ion irradiation damage in FeCr alloys, J Nucl Mater 386 (2009) 161-164.
- [34] R. Schäublin, B. Décamps, A. Prokhodtseva, J.F. Löffler, On the origin of primary ½ a0< 111> and a0< 100> loops in irradiated Fe (Cr) alloys, Acta Materialia 133 (2017) 427-439.
- [35] X. Wang, N. Gao, Y. Wang, X. Wu, G. Shu, C. Li, Q. Li, B. Xu, W. Liu, Formation of (100) dislocation loop in bcc-Fe via the ternary loop reaction, Scripta Mater 162 (2019) 204-208.
- [36] J. Byggmästar, F. Granberg, A. Sand, A. Pirttikoski, R. Alexander, M. Marinica, K. Nordlund, Collision cascades overlapping with self-interstitial defect clusters in Fe and W, Journal of Physics: Condensed Matter 31(24) (2019) 245402.
- [37] F. Granberg, J. Byggmästar, K. Nordlund, Cascade overlap with vacancy-type defects in Fe, The European Physical Journal B 92(7) (2019) 146.
- [38] A. Fellman, A. Sand, J. Byggmästar, K. Nordlund, Radiation damage in tungsten from cascade overlap with voids and vacancy clusters, Journal of Physics: Condensed Matter 31(40) (2019) 405402.
- [39] D. Terentyev, K. Vörtler, C. Björkas, K. Nordlund, L. Malerba, Primary radiation damage in bcc Fe and Fe–Cr crystals containing dislocation loops, J Nucl Mater 417(1-3) (2011) 1063-1066.
- [40] L.K. Béland, Y.N. Osetsky, R.E. Stoller, H. Xu, Interstitial loop transformations in FeCr, Journal of Alloys and Compounds 640 (2015) 219-225.
- [41] S. Plimpton, Fast Parallel Algorithms for Short-Range Molecular-Dynamics, J Comput Phys 117(1) (1995) 1-19.
- [42] A. Stukowski, B. Sadigh, P. Erhart, A. Caro, Efficient implementation of the concentration-dependent embedded atom method for molecular-dynamics and Monte-Carlo simulations, Model Simul Mater Sc 17(7) (2009).
- [43] A. Stukowski, B. Sadigh, P. Erhart, A. Caro, Efficient implementation of the concentration-dependent embedded atom method for molecular-dynamics and Monte-Carlo simulations, Model Simul Mater Sc 17(7) (2009) 075005.
- [44] Y. Zhang, D. Schwen, X.-M. Bai, Molecular dynamics simulations of concentration-dependent defect production in Fe-Cr and Fe-Cu alloys, J Appl Phys 122(22) (2017) 225902.
- [45] P. Olsson, I. Abrikosov, J. Wallenius, Electronic origin of the anomalous stability of Fe-rich bcc Fe-Cr alloys, Phys Rev B 73(10) (2006) 104416.
- [46] D. Nguyen-Manh, A. Horsfield, S. Dudarev, Self-interstitial atom defects in bcc transition metals: Group-specific trends, Phys Rev B 73(2) (2006) 020101.
- [47] P. Olsson, C. Domain, J. Wallenius, Ab initio study of Cr interactions with point defects in bcc Fe, Phys Rev B 75(1) (2007) 014110.
- [48] M. Mendelev, S. Han, D. Srolovitz, G. Ackland, D. Sun, M. Asta, Development of new interatomic potentials appropriate for crystalline and liquid iron, Philos Mag 83(35) (2003) 3977-3994.
- [49] G. Bonny, R.C. Pasianot, D. Terentyev, L. Malerba, Iron chromium potential to model high-chromium ferritic alloys, Philos Mag 91(12) (2011) 1724-1746.

- [50] Y. Zhang, D. Schwen, X.-M. Bai, Effects of Solute-SIA binding energy on defect production behaviors in Fe-based alloys, J Nucl Mater 509 (2018) 124-133.
- [51] J.F. Ziegler, J.P. Biersack and U. Littmark, The stopping and range of ions in solids, in The Stopping and Range of Ions in Matter, J.F. Ziegler, ed., Pergamon, New York (1985).
- [52] A. Stukowski, Visualization and analysis of atomistic simulation data with OVITO-the Open Visualization Tool, Model Simul Mater Sc 18(1) (2009) 015012.
- [53] A. Stukowski, V.V. Bulatov, A. Arsenlis, Automated identification and indexing of dislocations in crystal interfaces, Modelling Simulation in Materials Science Engineering 20(8) (2012) 085007.
- [54] A. Stukowski, K. Albe, Extracting dislocations and non-dislocation crystal defects from atomistic simulation data, Model Simul Mater Sc 18(8) (2010) 085001.
- [55] R.E. Stoller, The influence of PKA direction on displacement cascade evolution, MRS Online Proceedings Library Archive 650 (2000).
- [56] X.-M. Bai, A.F. Voter, R.G. Hoagland, M. Nastasi, B.P. Uberuaga, Efficient annealing of radiation damage near grain boundaries via interstitial emission, Science 327(5973) (2010) 1631-1634.
- [57] G. Ackland, M. Mendelev, D. Srolovitz, S. Han, A. Barashev, Development of an interatomic potential for phosphorus impurities in α -iron, Journal of Physics: Condensed Matter 16(27) (2004) S2629.
- [58] L. Malerba, M.-C. Marinica, N. Anento, C. Björkas, H. Nguyen, C. Domain, F. Djurabekova, P. Olsson, K. Nordlund, A. Serra, Comparison of empirical interatomic potentials for iron applied to radiation damage studies, J Nucl Mater 406(1) (2010) 19-38.
- [59] J. Byggmästar, F. Granberg, K. Nordlund, Effects of the short-range repulsive potential on cascade damage in iron, J Nucl Mater 508 (2018) 530-539.
- [60] W.-Y. Chen, Y. Miao, J. Gan, M.A. Okuniewski, S.A. Maloy, J.F. Stubbins, Neutron irradiation effects in Fe and Fe-Cr at 300° C, Acta Materialia 111 (2016) 407-416.
- [61] G. Bonny, N. Castin, J. Bullens, A. Bakaev, T. Klaver, D. Terentyev, On the mobility of vacancy clusters in reduced activation steels: an atomistic study in the Fe–Cr–W model alloy, Journal of Physics: Condensed Matter 25(31) (2013) 315401.
- [62] M.I. Mendelev, S. Han, W.-j. Son, G.J. Ackland, D.J. Srolovitz, Simulation of the interaction between Fe impurities and point defects in V, Phys Rev B 76(21) (2007) 214105.
- [63] D. Smirnova, A.Y. Kuksin, S. Starikov, V. Stegailov, Z. Insepov, J. Rest, A. Yacout, A ternary EAM interatomic potential for U–Mo alloys with xenon, Model Simul Mater Sc 21(3) (2013) 035011.
- [64] Y. Zhang, R. Ashcraft, M. Mendelev, C. Wang, K. Kelton, Experimental and molecular dynamics simulation study of structure of liquid and amorphous Ni62Nb38 alloy, The Journal of chemical physics 145(20) (2016) 204505.
- [65] R. Ravelo, T. Germann, O. Guerrero, Q. An, B. Holian, Shock-induced plasticity in tantalum single crystals: Interatomic potentials and large-scale molecular-dynamics simulations, Phys Rev B 88(13) (2013) 134101.

- [66] E. Wakai, A. Hishinuma, Y. Kato, H. Yano, S. Takaki, K. Abiko, Radiation-induced α'phase formation on dislocation loops in Fe-Cr alloys during electron irradiation, Le Journal de Physique IV 5(C7) (1995) C7-277-C7-286.
- [67] K. Bawane, K. Lu, X.-M. Bai, W.-Y. Chen, M. Li, In-situ TEM study of microstructural evolution in NFA and Cr3C2@ SiC-NFA composite during ion irradiation, Materialia 7 (2019) 100412.